Original article

Microscopic remaining oil distribution and quantitative analysis of polymer flooding based on CT scanning

Xin Wang[1], Hongwei Yin[2], Xia Zhao[3], Bingxian Li[3], Yongfei Yang[1]*

[1]*Research Center of Multiphase Flow in Porous Media, School of Petroleum Engineering, China University of Petroleum (East China), Qingdao 266580, P. R. China*

[2] *Kela Oil and Gas Development Department, PetroChina Tarim Oilfield Company, Korla 841000, P. R. China*

[3]*Marine Oil Production Plant, Sinopec Shengli Oilfield, Dongying 257237, P. R. China*

Abstract:
To investigate the distribution characteristics of remaining oil after polymer flooding, the core samples of different stages of water flooding and polymer flooding were scanned and imaged based on CT scanning technology. The oil, water and rock were divided into three phases by image analysis method, and the corresponding digital cores were constructed. Through the qualitative and quantitative analysis of the two-dimensional image and three-dimensional structure at the same position, the quantitative characterization of the micro-residual oil distribution in different displacement stages is finally realized. The results show that, the polymer flooding can significantly improve the sweep efficiency, which can increase the oil recovery by 11.45% compared with water flooding. The remaining oil in the pore is mainly network and multiple, and mainly network distribution at the stage of water flooding. After adding polymer, the proportion of multiple remaining oil increases significantly and becomes the main occurrence state of remaining oil. Affected by Jamin effect, multiple residual oil in the pore is difficult to be recovered because it cannot pass through the throat. The radius of this part of remaining oil is usually 1.34~1.5 times that of the throat radius.

1. Introduction

Polymer flooding is usually used in oilfields to increase affected area and improve oil displacement efficiency (Wang et al., 2005; Clarke et al., 2016). However distribution of remaining oil in affected area is usually very complex (Lu et al., 1996; Sun et al., 2018). Therefore, it is very important to know the distribution of remaining oil in the flooding affected area for further improving the recovery of remaining oil after polymer flooding (Li et al., 2017). Researchers have used numerical simulation method (Dalla et al., 2002; Bryant et al., 2004; Raeini et al., 2015; Golparvar et al. 2018) and two-dimensional model (Sahloul et al., 2002; Chen et al., 2007; Hossein et al., 2013; Zhou et al., 2014) to simulate multiphase flow to study the displacement mechanism of different displacement fluids and predict the distribution of remaining oil. However, these methods are uncertain because they do not consider the pore structure characteristics of real cores. In recent years, with the introduction of a number of high-tech imaging equipment into the petroleum industry, it

is possible to study the occurrence pattern of remaining oil at the pore scale. For example, Researchers have used nuclear magnetic resonance (NMR) to study the distribution of oil and water in cores, and shown that the distribution of remaining oil is closely related to the pore structure characteristics (Yang et al., 2013; Ge et al., 2018).

With its advantages of high accuracy and nondestructive imaging, X-ray micro-computed tomography (micro CT) has become an excellent method for capturing pore structure and residual fluids in reservoir rocks (Armstrong et al., 2014). Micro CT uses X-ray to irradiate samples (Guo et al., 2018; Gu et al., 2019). Because the density of different components in the samples is different, the absorption degree of X-ray is different. Thus, two-dimensional or three-dimensional gray images can be generated by attenuation degree of X-ray and image reconstruction algorithm (Kak and Slaney., 2002). Although the distribution of various substances can be observed directly from CT images, the basic parameters cannot be calculated directly and quantitatively. Therefore,
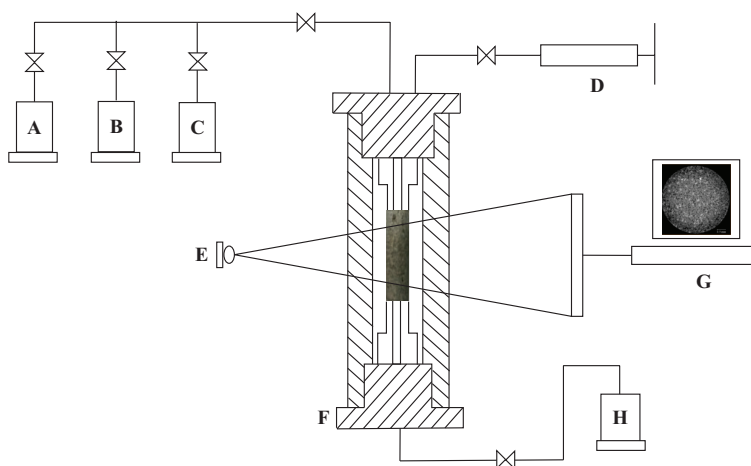
Fig. 1. In-situ micro CT core flooding apparatus. Core flooding system: (A) brine injection pump, (B) oil injection pump, (C) polymer injection pump, (D) hand pump, (E) micro CT, (F) X-ray transparent core holder assembly, (G) micro CT image processing, (H) reflux pump.

researchers usually use CT images to construct digital cores, which is one of the most accurate methods to construct digital cores (Yao et al., 2015; Liu et al., 2017). Digital core is a good carrier to analyze pore size, shape and connectivity (Yang et al., 2015; Yang et al., 2016). Using digital core, it is possible to identify and measure fractures (Vandersteen et al., 2003; Yang et al., 2017). Recently, many other applications of digital core in studying the displacement effect and quantitatively characterizing the distribution of remaining oil have been presented (Kumar et al., 2010; Georgiadis et al., 2013; Rücker et al., 2015). In addition, digital core can also predict core permeability through numerical simulation method (Beckingham et al., 2013; Song et al., 2016; Chen et al., 2018).

At the end of displacement of oil-bearing reservoirs, a considerable amount of remaining oil is retained in the affected area. Understanding the micro-distribution of remaining oil in reservoir rock pore space is of great significance to better understand the mechanism of reservoir exploitation and design tertiary oil recovery technology. Although the pore size structure and remaining oil distribution are very important, there are few studies on the relationship between remaining oil distribution and reservoir pore structure. In this paper, we used CT scanning and digital core method to study the displacement mechanism of polymer flooding and the distribution of remaining oil after polymer flooding. Then we quantitatively characterized the micro-occurrence state of remaining oil, which could provide a theoretical basis for further improving oil recovery.

2. Experimental materials and methods

2.1 Materials and equipment

The core of this experiment comes from a natural sandstone. The porosity of the core is 29.1%, and the gas permeability is 500 mD, which is a middle permeability sandstone core. In the experiment, the core should be placed in a special carbon fiber core holder. The diameter and length of the core

are 9.8 mm and 21.8 mm, respectively. The experimental oil is composed of crude oil and kerosene in a ratio of 1:1, and its viscosity is 2.6 mPa·s measured at 20 °C. The injected water used in saturated cores and displacement is potassium iodide brine with 10% mass fraction. The potassium iodide has strong X-ray absorption ability and can obviously improve the image contrast between water and oil. The component of the polymer used in the experiment is partially hydrolyzed polyacrylamide. The concentration of the prepared polymer solution is 800 mg/L, and its viscosity is 6.7 mPa·s measured at 20 °C.

The main instruments of this experiment are advection pump, carbon fiber core holder, micro XCT-400 micron CT and Avizo image processing software (Fig. 1).

2.2 Experimental steps

(1) The oil-washed and fully dried core was placed in the core holder for the first CT scan. (2) The dry core was vacuumed for 24 hours and then saturated the water. (3) The core was then flooded with oil at 2 MPa pore pressure. The confining pressure was applied by water with a high precision hand pump. The core was then micro CT imaged after resting for 24 hours to simulate the reservoir formation process. (4) The core was then flooded with brine under a confining pressure of 2 MPa. The third and fourth groups of CT images were obtained by CT scanning at the 1 PV and 15 PV stages of water flooding respectively. (5) The polymer slug with 0.5 PV configuration was injected and then water flooding was carried out again. CT scans were carried out at the 1 PV and 15 PV stages respectively. The fifth and sixth groups of CT images were obtained. (6) The image analysis was processed.

The core holder was kept fixed in CT during the whole experiment. In the displacement experiment, we shut down the X-ray source, connected the pipeline to the core holder and started the displacement experiment. After displacement, the pipeline was removed and the core holder was stationed
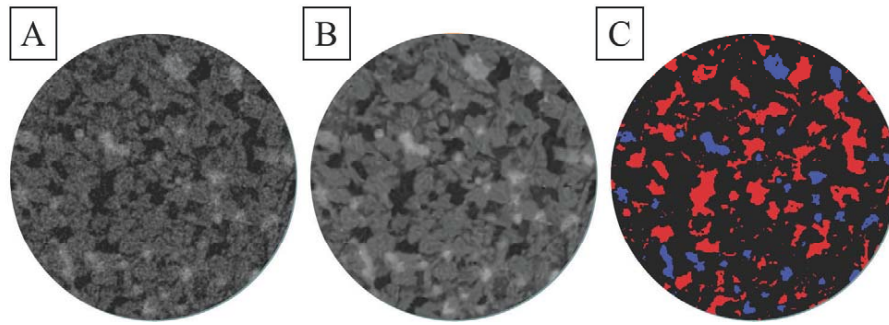
Fig. 2. 2D slices of saturating oil in core. (A) original gray scale image, black is oil, white is water and gray is rock; (B) image after applying by non-local means filter; (C) image after applying by watershed segmentation, red is oil, blue is water and black is rock.

for 1 hour to ensure the stability of the fluid in the core so as to obtain a clear CT image(Yang et al., 2019). It takes about 4 hours for a single CT scan and the image resolution is 4.18 μm.

2.3 Image processing

The original CT image cannot be directly used for oil-water phase recognition. We need to use some image processing software to process the CT image to obtain the relevant data for analysis.

Due to the influence of equipment and experimental environment, a lot of noise usually appears in CT images, which makes the phase boundary unclear. Filtering can remove the noise in the image. Non-local mean filter is a popular filtering method in recent years. It can effectively improve the signal-to-noise ratio of the image, while maintaining a clear the general steps of image processing include intercepting the representative elementary volume (REV), filtering and image segmentation, as shown in Fig. 2. REV is a subunit which is intercepted from any position in the original 3D data. It is required that the unit body should be as small as possible while ensuring that its physical properties are consistent with those of the whole core. It can effectively improve the computational efficiency and save computer computing resources. Meanwhile we can keep the same position of each interception to study the distribution of oil and water at the same position in the core at different displacement times, and realize the 4D observation of the dynamic distribution of remaining oil. The size of REV is very important for the reliability of experimental analysis results. Some studies show that the porosity can be well characterized when the REV size is larger than 400 μm, and the permeability can be characterized when the REV size is larger than 800 μm (Mostaghimi et al., 2013). Some researchers also found that when the REV grid size is 300 $\times$ 300 $\times$ 300, it can characterize the porosity and permeability characteristics of sandstone and be used in oil-water two-phase displacement simulation (Gao et al., 2014). In this paper, the grid size of the REV is 300 $\times$ 300 $\times$ 300, and its actual physical size is 1254 μm $\times$ 1254 μm $\times$ 1254 μm. and smooth interface between two phases. This will improve the accuracy of segmentation, so that the experimental results are more reliable.

In this paper, watershed segmentation method was used to segment the image (Yang et al., 2016). Image segmentation is based on the gray scale image of CT image. Substances with the same properties have the same gray level in CT images, which will form a peak in the gray distribution. The minimum value of the gray distribution frequency between the two peaks is the segmentation threshold. By choosing the segmentation threshold, the phase substances in the image are segmented and recognized.

2.4 Pore network model (PNM)

Pore network model uses simple and regular geometric shape to replace complex pore space, which could quantitatively analyze the geometric and topological characteristics of pore (Yancy-Caballero et al., 2019; Song et al., 2020). The 3D digital core consists of a series of pixels. To extract the pore network model, we need to extract the distance feature from each target pixel to the boundary and identify the categories of various groups of pixels by distance feature (Jiang et al., 2007). We use Euclidean distance formula to find the minimum distance from each target pixel to the boundary, which is defined as Eq. (1):

$$d_E(p,q) = \sqrt{(x_1 - x_2)^2 + (y_1 - y_2)^2 + (z_1 - z_2)^2} \quad (1)$$

where $d_E(p,q)$ represents the Euclidean distance between points p and q. x, y, z are their coordinate positions. Each target pixel is assigned its own minimum Euclidean distance value, thus a new "distance gray image" can be obtained. Finally, the pore and throat can be identified by segmentation.

3. Results and discussion

3.1 Analysis of pore structure characteristics

We quantitatively analyzed the pore structure characteristics of dry core based on the digital core and pore network model (Fig. 3).

Fig. 4 shows that the pore radius distribution of the core has multiple peaks, while the peak pore radius appears in the range of 11~19 μm with an average pore radius of 15.4 μm. Throat radius is mainly distributed between 5 and 14 μm with
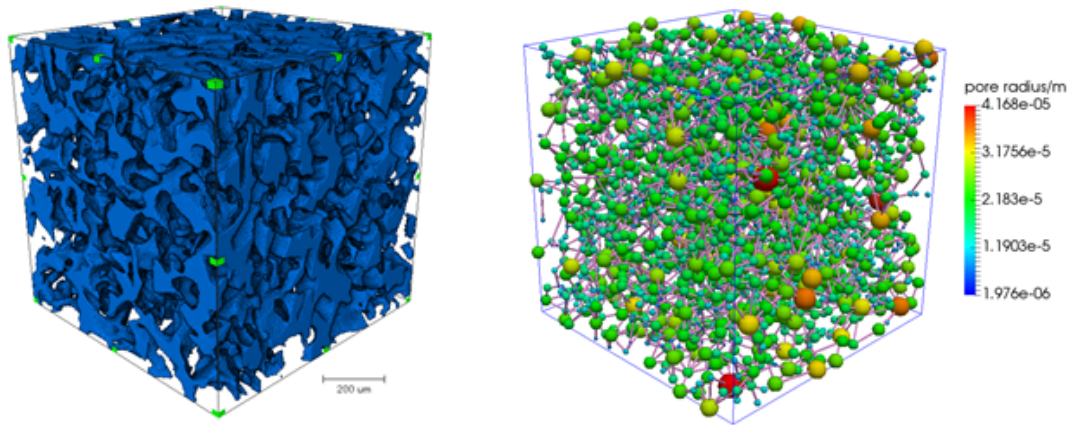
Fig. 3. 3D digital core and pore network model of dry core.

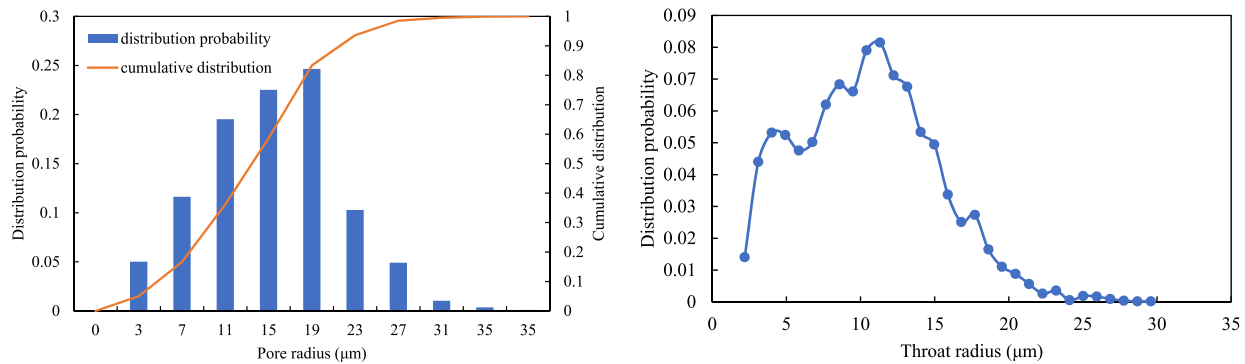**Fig. 4.** Frequency distribution of pore and throat radius.

an average throat radius of 10.5 μm. The wide distribution of pore and throat radius indicates that the core has strong heterogeneity. The pore structure of the core is complex while a large number of mesoporosity, fine pore and throats are developed.

3.2 Analysis of displacement experiment results

The image processing results of different displacement stages are shown in Table 1. After obtaining the three-dimensional distribution view of micro remaining oil, we analyzed the relevant information of remaining oil data, including the number, volume, remaining oil saturation and displacement efficiency of remaining oil. The statistical results are shown in Table 2.

From 2D slices, after saturating oil is completed, oil is distributed in different pore sizes, while water is mainly distributed in small pore sizes. In the early stage of water flooding, the water phase occupies the mesoporosity preferentially and forms the dominant channel, while the remaining oil in the macroporosity or fine pore is not displaced obviously. Remaining oil in macroporosity is due to the large resistance caused by Jamin effect when large oil drops pass through narrow throat. When driving force is insufficient to overcome

resistance, these remaining oil is not easy to be displaced. Because of the strong heterogeneity of the core, water fingering occurs during displacement and the remaining oil in the small pore cannot be affected by water.

From the displacement effect, the displacement effect in the early stage of water flooding is also the best. The recovery efficiency at 1 PV of water flooding can account for 67.47% of the total recovery efficiency of water flooding. By the end of water flooding, the final recovery efficiency is only 43.35%. After water flooding, the remaining oil in the small pore is basically not recovered, while the oil in the macropore is divided into several blocks by water, which remains in the corner of the pore. As a result, the number of isolated remaining oil blocks in water flooding stage increases greatly and the distribution of remaining oil in pore is more complex.

After adding polymer slug, the affecting range of subsequent water flooding increases obviously because the polymer blocked part of the high permeability channel. Therefore, it can be seen from the 2D slice image that the amount of remaining oil in the small pore obviously decreases at this stage. On the other hand, due to the viscoelastic effect of polymer, the remaining oil distributed in the corner is recoalesced in the pore. Therefore, after injection of polymer, the number of remaining oil blocks decreases significantly,
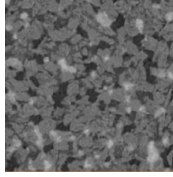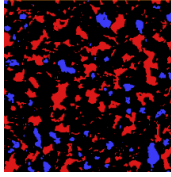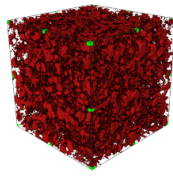
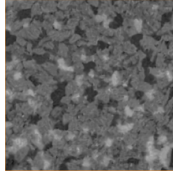**Table 1.** CT images of different displacement stages.
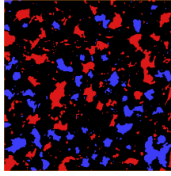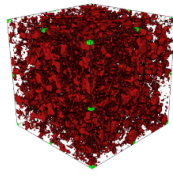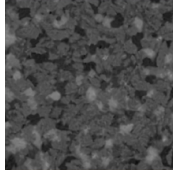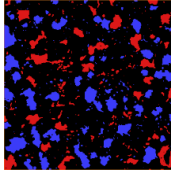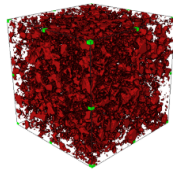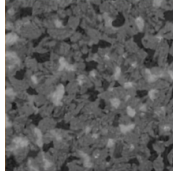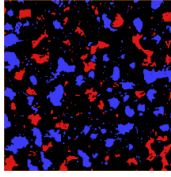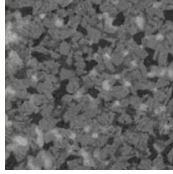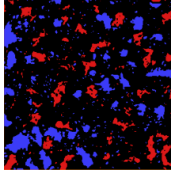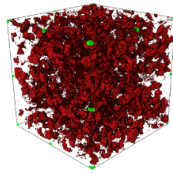
Displacement stage	Filtered image	Segmentation image	3D image of oil phase
Saturating oil			
Water flooding 1PV			
Water flooding 15PV			
Polymer flooding 1PV			
Polymer flooding 15PV			

Table 2. Quantitative characterization of remaining oil.

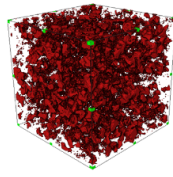| Displacement stage	Oil saturation (%)	Number of oil clusters	Average volume of oil clusters (μm^3)	Recovery ratio (%)
Saturating oil	79.62	7269	53344.5	0
Water flooding 1 PV	56.33	9555	27691.5	29.25
Water flooding 15 PV	45.11	10572	20261.7	43.35
Polymer flooding 1PV	41.84	9411	21137.1	47.45
Polymer flooding 15PV	35.99	8711	19519	54.80

Table 3. Classification basis of remaining oil occurrence form.

Types of remaining oil	Scope of shape factor value	Range of contact area ratio
Singlet	$G>0.3$	$0<C<1$
	$0.1<G<0.3$	$C<0.45$ or $C>0.6$
Film	$0.1<G<0.3$	$0.45<C<0.6$
Multiple	$0.01<G<0.1$	$0<C<1$
Network	$G<0.01$	$0<C<1$

Table 4. Proportion of different remaining oil occurrence forms.

Displacement stage	Network (%)	Multiple (%)	Singlet(%)	Film (%)
Saturating oil	96.22	3.5	0. 17	0. 11
Water flooding 1 PV	84.91	14.57	0. 31	0. 21
Water flooding 15 PV	55.34	43.93	0. 46	0. 27
Polymer flooding 1 PV	18.58	80.7	0. 46	0.26
Polymer flooding 15 PV	28.39	70.81	0. 51	0.29
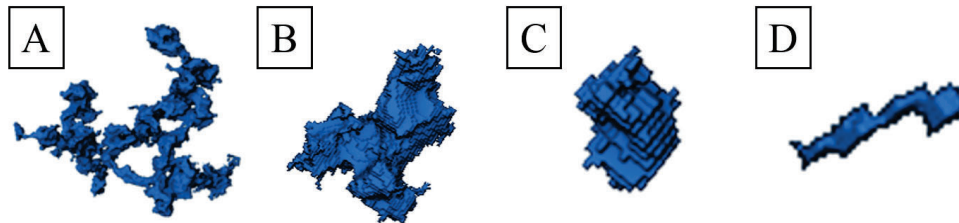
Fig. 5. Quantitative characterization of remaining oil. (A) network; (B) multiple; (C) singlet; (D) film.

which indicates that polymer can improve the occurrence of remaining oil in the pore and provide convenience for the next step of stimulation measures. The ultimate recovery efficiency of polymer flooding is 54.80%, which is 11.45% higher than that of water flooding. The effect of enhancing oil recovery is obvious but nearly half of the remaining oil has not been recovered.

3.3 Quantitative characterization of remaining oil occurrence

The occurrence patterns of remaining oil in pore is complex and varied. Generally, we can divide the remaining oil into network, multiple, singlet and oil film according to its shape, size and contact with skeleton. Specific criteria are listed in Table 3 (Hou et al., 2014).

Shape factor is a parameter representing the relationship between the volume and area of oil clusters. It is defined as Eq. (2).

$$G = 6\frac{\sqrt{\pi}V}{S^{1.5}} \tag{2}$$

where G is shape factor, V is volume of single oil cluster, μm^3, S is surface area of single oil cluster, μm^2. The smaller the shape factor, the more complex the remaining oil is. The contact area ratio is the ratio of the remaining oil to the rock contact area and the remaining oil surface area. It is mainly used to distinguish between solitary and oil-film remaining oil. The area ratio of oil film remaining oil is about 0.5 because one surface is attached to the skeleton surface. According to the shape factor and the contact area ratio, the occurrence patterns of remaining oil can be classified, as shown in Fig. 5.

Table 4 shows the distribution proportion of different remaining oil occurrence patterns in each displacement stage. Most of the remaining oil occurrence patterns are network

and multiple. However their proportion varies greatly. The number of singlet and oil film remaining oil is very large. The proportion of oil film and singlet remaining oil is small, both less than 1%, because the volume of single remaining oil is too small, which has no potential to be developed.

During the saturating oil stage, oil distributes continuously in the pore and network is the main occurrence patterns of oil phase. In water flooding stage, the oil in the high permeability channel is first driven and these channels are occupied by water phase. Oil, as continuous phase, is separated by water, resulting in a continuous decline in the proportion of network remaining oil. However, the remaining oil after water cutting mostly exists in the form of multiple remaining oil, so it can be seen that the proportion of multiple remaining oil in the pore increases significantly. After water flooding, the proportion of network remaining oil is slightly more than that of multiple remaining oil. In the polymer flooding stage, after polymer blocking the high permeability channel, a large number of remaining oil in the low permeability area is driven. The continuous distribution of oil phase is constantly blocked by water. The proportion of network remaining oil is sharply reduced and the remaining oil is mainly multiple distribution. In the late stage of polymer flooding, due to the viscoelastic effect of polymer, some multiple remaining oil is re-aggregated to form network remaining oil. Although the proportion of network remaining oil has risen, multiple remaining oil has become the main form of remaining oil.

3.4 Quantitative characterization of remaining oil size

From the above section, it can be seen that after polymer flooding, the main occurrence form of remaining oil changes from network to multiple. In order to study the occurrence size of these multiple remaining oil in the pore, we extracted the pore network model of the remaining oil in each displacement

Fig. 6. Pore network model of remaining oil in different displacement stages. (A) oil saturated; (B) water flooding 1 PV; (C) water flooding 15 PV; (D) polymer flooding 1 PV; (E) polymer flooding 15 PV.
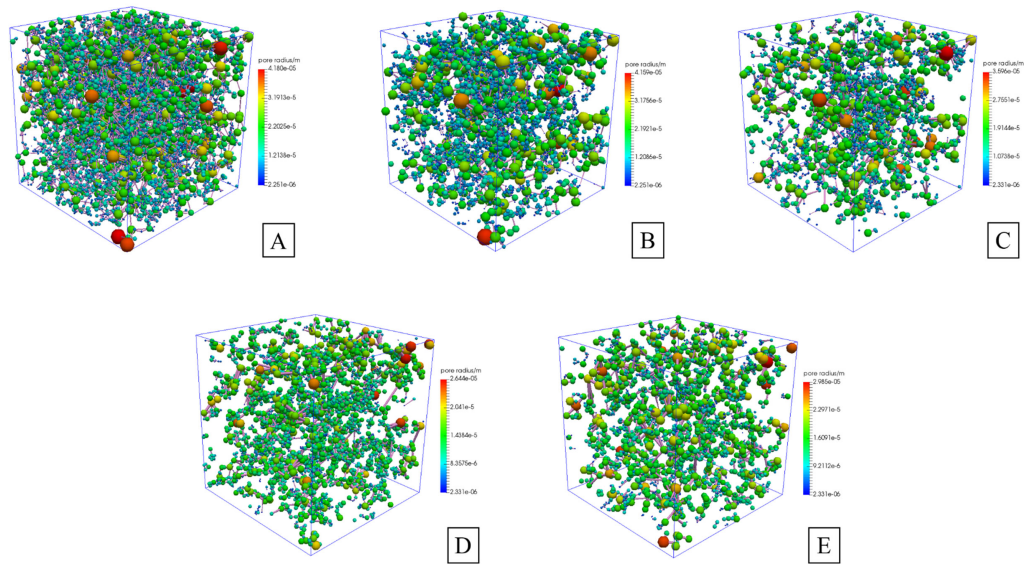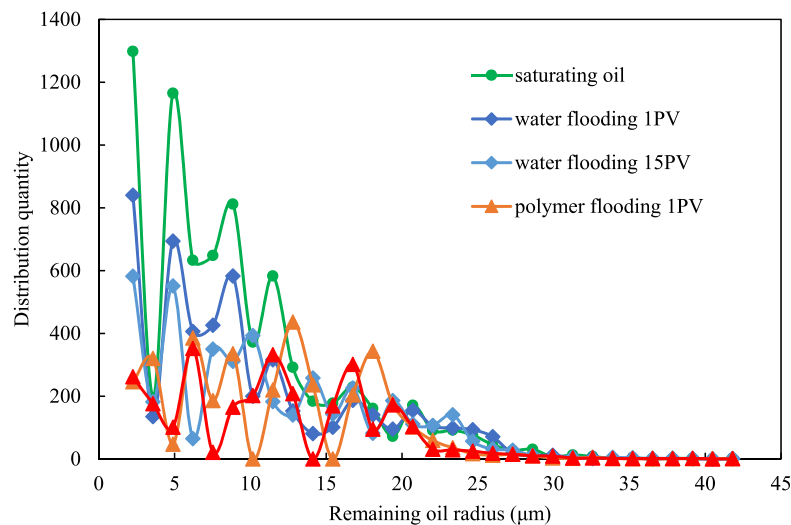

Fig. 7. Distribution of remaining oil occurrence in different displacement stages.

stage (Fig. 6) and then quantitatively studied their occurrence size in the pore. The occurrence size of remaining oil in pore is closely related to throat radius, as shown in Fig. 7.

After adding polymer slug, the amount of remaining oil with radius less than 10.5 μm (average throat radius) decreased significantly, which indicated that the polymer had a good ripple effect on remaining oil distributed in small pore and fine throat. In addition, in the early stage of adding polymer slug, the remaining oil distributed in the corner re-aggregates in the pore and forms larger remaining oil due to the influence of polymer viscoelasticity. Thus, it can be seen in the figure that there are several obvious peaks in the radius distribution of remaining oil when polymer flooding is 1 PV and the radius of remaining oil corresponding to the peak is larger than that of water flooding. However, with the development

of polymer flooding, the remaining oil is cut again by water. Some of remaining oil are displaced and the others remain in the pore. Up to the end of displacement, the radius distribution of remaining oil in pore is mainly concentrated at 6, 11.5 and 17 μm. Considering the distribution of throat radius of the core, there are also three peaks, 4, 8.58 and 11.32 μm, respectively. Therefore, we think that the remaining oil is trapped in the pore because it can't pass through these narrow throats. Finally, we calculate the ratio of the radius of the remaining oil to the radius of the throat which it could not pass, and find that the ratio is 1.34~1.5.

4. Conclusion

The distribution of oil and water in core pore can be observed by in-situ CT scanning technology. At the same time,

the 4D quantitative analysis of remaining oil distribution can be realized by intercepting the REV at the same location. The ultimate recovery factor of water flooding is 43.35%. During this stage, the number of remaining oil clusters increases, the network remaining oil changes to multiple remaining oil and the remaining oil in pore becomes more complex. Compared with water flooding, polymer flooding can improve oil recovery by 11.45%, while ultimate oil recovery is 54.80%. In addition, the influence of polymer viscoelasticity and the improvement of sweep coefficient of displacement greatly reduce the number of remaining oil clusters. Polymer flooding can make the remaining oil more concentrated in the pore, which could facilitate the implementation of subsequent stimulation measures.

The remaining oil in the pore is mainly network and multiple. With the development of displacement, the network remaining oil gradually changes to multiple remaining oil. By the end of polymer flooding, the proportion of multiple remaining oil in the pores is 70.81%. These multiple remaining oil is usually due to additional resistance caused by Jamin effect, which prevents them from passing through the throat. The radius of these remaining oil is usually 1.34~1.5 times bigger than that of the throat radius. It is suggested that surfactant flooding should be carried out after polymer flooding to reduce the interfacial tension between oil and water, so as to reduce the influence of Jamin effect and make the remaining oil with larger radius pass through throat.

Acknowledgments

References

Armstrong, R.T., Ott, H., Georgiadis, A., et al. Subsecond pore-scale displacement processes and relaxation dynamics in multiphase flow. Water Resour. Res. 2014, 50(12): 9162-9176.

Beckingham, L.E., Peters, C.A., Um, W., et al. 2D and 3D imaging resolution trade-offs in quantifying pore throats for prediction of permeability. Adv. Water Resour. 2013, 62(a): 1-12.

Bryant, S.L., Anna, J. Bulk and film contributions to fluid/fluid interfacial area in granular media. Chem. Eng. Commun. 2004, 191(12): 1660-1670.

Chen, D., Pyrak-Nolte, L.J., Griffin, J., et al. Measurement of interfacial area per volume for drainage and imbibition. Water Resour. Res. 2007, 43(12): W12504.

Chen, X., Verma, R., Espinoza, D.N., et al. Pore-scale determination of gas relative permeability in hydrate-bearing sediments using x-ray computed micro-tomography and lattice boltzmann method. Water Resour. Res. 2018, 54(1): 600-608.

Clarke, A., Howe, A.M., Mitchell, J., et al. How viscoelastic-polymer flooding enhances displacement efficiency. SPE J. 2016, 21(3): 675-687.

Dalla, E., Hilpert, M., Miller, C.T. Computation of the interfacial area for two-fluid porous medium systems. J. Contam. Hydrol. 2002, 56(1-2): 25-48.

Gao, Y., Yao, J., Yang, Y., et al. REV identification of tight sandstone in sulige gas field in changqing oilfield china using CT based digital core technology. Paper SCA2014-036 Presented at 2014 International Symposium of the Society of Core Analysts, Avignon, France, 8-11 September, 2014.

Georgiadis, A., Berg, S., Makurat, A., et al. Pore-scale micro-computed-tomography imaging: nonwetting-phase cluster-size distribution during drainage and imbibition. Phys. Rev. E. 2013, 88(3): 033002.

Ge, X., Liu, J., Fan, Y., et al. Laboratory investigation into the formation and dissociation process of gas hydrate by low-field NMR technique. J. Geophys. Res: Solid Earth 2018, 123(5): 3339-3346.

Golparvar, A., Zhou, Y., Wu, K., et al. A comprehensive review of pore scale modeling methodologies for multiphase flow in porous media. Adv. Geo-energ. Res. 2018, 2(4): 418-440.

Guo, C., Wang, X., Wang, H., et al. Effect of pore structure on displacement efficiency and oil-cluster morphology by using micro computed tomography (μCT) technique. Fuel 2018, 230: 430-439.

Gu, X., Pu, C., Khan, N., et al. The visual and quantitative study of remaining oil micro-occurrence caused by spontaneous imbibition in extra-low permeability sandstone using computed tomography. Fuel 2019, 237: 152-162.

Hou, J., Qiu, M., Lu, N., et al. Characterization of residual oil microdistribution at pore scale using computerized tomography. Acta Petrolei Sinica 2014, 35(2): 319-325 (in Chinese).

Jiang, Z., Wu, K., Couples, G., et al. Efficient extraction of networks from three-dimensional porous media. Water Resour. Res. 2007, 43(13): W12S03.

Kak, A.C., Slaney, M. Principles of computerized tomographic imaging. Med. Phys. 2002, 29(1): 107-107.

Kumar, M., Knackstedt, M.A., Senden, T.J., et al. Visualizing and quantifying the residual phase distribution in core material. Petrophysics 2010, 51(5): 323-332.

Li, J., Jiang, H., Wang, C., et al. Pore-scale investigation of microscopic remaining oil variation characteristics in water-wet sandstone using CT scanning. J. Nat. Gas Sci. Eng. 2017, 48: 36-45.

Liu, Z., Yang, Y., Yao, J., et al. Pore-scale remaining oil distribution under different pore volume water injection based on CT technology. Adv. Geo-energ. Res. 2017, 1(3): 171-181.

Lu, X., Gao, Z., Zhao, X., et al. Distribution regularities of remaining oil in heterogeneous reservoirs after polymer flooding. Acta Petrolei Sinica 1996, 17(4): 55-61 (in

Chinese).

Mostaghimi, P., Blunt, M.J., Bijeljic, B. Computations of absolute permeability on micro-CT images. Math. Geosci. 2013, 45(1): 103-125.

Raeini, A.Q., Bijeljic, B., Blunt, M.J. Modelling capillary trapping using finite-volume simulation of two-phase flow directly on micro-CT images. Adv. Water Resour. 2015, 83: 102-110.

Rücker, M., Berg, S., Armstrong, R., et al. From connected pathway flow to ganglion dynamics. Geophys. Res. Lett. 2015, 42(10): 3888-3894.

Sahloul, N., Ioannidis, M., Chatzis, I. Dissolution of residual non-aqueous phase liquids in porous media: Pore-scale mechanisms and mass transfer rates. Adv. Water Resour. 2002, 25(1): 33-49.

Song, W., Yao, J., Wang, D., et al. Dynamic pore network modelling of real gas transport in shale nanopore structure. J. Pet. Sci. Eng. 2020, 184: 106506.

Song, W., Yao, J., Li, Y., et al. Apparent gas permeability in an organic-rich shale reservoir. Fuel 2016, 181: 973-984.

Vandersteen, K., Busselen, B., Van Den Abeele, K., et al. Quantitative characterization of fracture apertures using microfocus computed tomography. Geol. Soc. Spec. Publ. 2003, 215(1): 61-68.

Wang, D., Cheng, J., Wu, J., et al. Application of polymer flooding technology in daqing oilfield. Acta Petrolei Sinica 2005, 25(1): 74-78 (in Chinese).

Yancy-Caballero, D., Ling, L.Y., Fujita, A., et al. Intraparticle connectivity in sugarcane bagasse unveiled by pore network modeling. Bioenerg. Res. 2019, 12: 546-557.

Yang, P., Guo, H., Yang, D. Determination of residual oil distribution during waterflooding in tight oil formations with NMR relaxometry measurements. Energ. Fuels 2013, 27(10): 5750-5756.

Yang, Y., Liu, Z., Sun, Z., et al. Research on stress sensitivity of fractured carbonate reservoirs based on CT technology. Energies 2017, 10(11): 1833.

Yang, Y., Yang, H., Tao, L., et al. Microscopic determination of remaining oil distribution in sandstones with different permeability scales using computed tomography scanning. J. Energ. Resour. Technol. 2019, 141(9): 092903.

Yang, Y., Yao, J., Wang, C., et al. New pore space characterization method of shale matrix formation by considering organic and inorganic pores. J. Nat. Gas Sci. Eng. 2015, 27(2): 496-503.

Yang, Y., Zhang, W., Gao, Y., et al. Influence of stress sensitivity on microscopic pore structure and fluid flow in porous media. J. Nat. Gas Sci. Eng. 2016, 36(a): 20-31.

Yao, J., Hu, R., Wang, C., et al. Multiscale pore structure analysis in carbonate rocks. Int. J. Multiscale Comput. Eng. 2015, 13(1): 1-9.

Zhou, Y., Helland, J., Hatzignatiou, D.G. Pore-scale modeling of waterflooding in mixed-wet-rock images: Effects of initial saturation and wettability. SPE J. 2014, 19(1): 88-100.